GeoHealth

RESEARCH ARTICLE

10.1029/2024GH001068

A New, Zero-Iteration Analytic Implementation of Wet-Bulb Globe Temperature: Development, Validation, and Comparison With Other Methods

Qinqin Kong[1] and **Matthew Huber**[1]

[1]Department of Earth, Atmospheric, and Planetary Sciences, Purdue University, West Lafayette, IN, USA

Key Points:

- Accurate wet-bulb globe temperature (WBGT) calculation, such as Liljegren's model, requires iteration
- By examining self-nonlinearities in Liljegren's model, we develop a simplified, analytic form—$\widehat{WBGT}$—that does not require iteration
- $\widehat{WBGT}$ is more accurate than commonly used simplified approximations, while retaining most of the physics in the Liljegren formulation

Correspondence to:

Q. Kong,
kong97@purdue.edu

Citation:

Kong, Q., & Huber, M. (2024). A new, zero-iteration analytic implementation of wet-bulb globe temperature: Development, validation, and comparison with other methods. *GeoHealth*, *8*, e2024GH001068. https://doi.org/10.1029/2024GH001068

Received 8 APR 2024
Accepted 8 SEP 2024

Abstract Wet-bulb globe temperature (WBGT)—a standard measure for workplace heat stress regulation—incorporates the complex, nonlinear interaction among temperature, humidity, wind and radiation. This complexity requires WBGT to be calculated iteratively following the recommended approach developed by Liljegren and colleagues. The need for iteration has limited the wide application of Liljegren's approach, and stimulated various simplified WBGT approximations that do not require iteration but are potentially seriously biased. By carefully examining the self-nonlinearities in Liljegren's model, we develop a zero-iteration analytic approximation of WBGT while maintaining sufficient accuracy and the physical basis of the original model. The new approximation slightly deviates from Liljegren's full model—by less than 1°C in 99% cases over 93% of global land area. The annual mean and 75%–99% percentiles of WBGT are also well represented with biases within ±0.5°C globally. This approximation is clearly more accurate than other commonly used WBGT approximations. Physical intuition can be developed on the processes controlling WBGT variations from an energy balance perspective. This may provide a basis for applying WBGT to understanding the physical control of heat stress.

Plain Language Summary Wet-bulb globe temperature (WBGT) is a standard way to measure heat stress in the workplace. It incorporates the complex, nonlinear interactive effects of temperature, humidity, wind and radiation. This complexity requires WBGT to be calculated iteratively which is computationally intensive and less straightforward to implement algorithmically. To address these issues, we came up with a simplified version of WBGT that obviates the need for iteration. This simplified approach is computationally straightforward and also highly accurate.

1. Introduction

Heat stress presents significant threats to human health (Buzan & Huber, 2020; Ebi et al., 2021; Kjellstrom et al., 2016) with wide-ranging social (Burke et al., 2018; Hsiang et al., 2013) and economic consequences (Burke et al., 2015; Saeed et al., 2022). Metrics that accurately represent the physiological impact of heat stress are crucial for the monitoring, early warning, and impact assessment of heat stress (Havenith & Fiala, 2015; Simpson et al., 2023).

Over the last century, numerous heat stress metrics have been formulated (de Freitas & Grigorieva, 2015), among which the wet-bulb globe temperature (WBGT) emerges as a notably comprehensive measure, encapsulating the interplay of temperature, humidity, wind speed and radiation effects (Yaglou & Minard, 1957). Rooted in physiology principles and fortified by empirical calibration, WBGT is as good or better than most other metrics in predicting human heat stress compensability (Vecellio et al., 2022), assessing the physiological influences of heat stress (Ioannou et al., 2022), and capturing the interactive effects of multiple meteorological factors on human physical work capacity (Foster et al., 2022a, 2022b; Havenith et al., 2024). It has been incorporated into several heat stress regulatory standards across various domains including occupational health (ISO, 2017; NIOSH, 2016; OSHA, 2017), military operations (Army, 2003) and athletic activities (ACSM, 1984). Nevertheless, WBGT has limitations, especially in its differing response to wind speed compared to humans (Budd, 2008; Foster et al., 2022a, 2022b; Havenith et al., 2024; Havenith & Fiala, 2015).

WBGT is defined as

$$WBGT = 0.7T_{nw} + 0.2T_g + 0.1T_a \quad (1)$$

under outdoor conditions where T_{nw}, T_g and T_a refer to natural wet-bulb temperature, black globe temperature and dry-bulb temperature respectively. The WBGT model developed by Liljegren et al. (2008) is the recommended approach for WBGT calculation due to its foundation on heat and mass transfer principles, careful treatment of the geometry of WBGT sensors, and extensive validation (RMSE <1°C) (Clark & Konrad, 2023; Lemke & Kjellstrom, 2012; Liljegren et al., 2008; Patel et al., 2013). It derives T_{nw} and T_g by solving the nonlinear energy balance equations of the wet wick and black globe sensors. However, this process requires iterative calculations which have limited the widespread adoption of Liljegren's approach. Even in recent work, a preference for simpler WBGT approximations that avoid iteration persists within the scientific community (e.g., Brimicombe et al., 2023; Kamal et al., 2024; Orlov et al., 2023; Tuholske et al., 2021; Zhu et al., 2021). However, these simplified approximations are so diverse in formulation that they generate substantially different estimates making the results from different studies challenging to meaningfully compare (Kong & Huber, 2022; Lemke & Kjellstrom, 2012). Some approximations are based on statistical relationship rather than physics (Australian Bureau of Meteorology, 2010; Kamal et al., 2024; Moran et al., 2001). The Australian Bureau of Meteorology WBGT formulation (hereafter referred as *sWBGT*) (Australian Bureau of Meteorology, 2010) has been demonstrated to be systematically biased, but remain widely used because of their simplicity (Kong & Huber, 2022). The generated heat stress estimates have been fed into impact models for assessing downstream social-economic consequences (Chavaillaz et al., 2019; de Lima et al., 2021; Matsumoto et al., 2021; Sun et al., 2024; Zhang & Shindell, 2021; Zhu et al., 2021). The propagation of biases stemming from these WBGT approximations through the chain of climate change impact assessment could potentially mislead policy-making pertaining to heat stress mitigation and adaptation.

We aim to address this issue by developing a simplified WBGT model that does not require iteration while maintaining sufficient accuracy and physics of heat and mass transfer. This is achieved with an analytic approximation of Liljegren's WBGT through substituting reasonable first-guess values of T_{nw} and T_g into the energy balance equations of the wet bulb and black globe sensors. The analytic approximation will be evaluated against Liljegren's full model which, although subject to biases compared to field observations (Clark & Konrad, 2023; Lemke & Kjellstrom, 2012; Liljegren et al., 2008; Patel et al., 2013), is treated as ground truth in this paper.

The remainder of this paper is structured as follows. Section 2 provides a concise overview of Liljegren's WBGT model focusing on the nonlinear energy balance equations. Section 3 introduces the analytic approximation of WBGT the accuracy of which is evaluated in Section 4. This evaluation is first conducted with synthetic data to understand the bias structure across the multidimensional parameter space encompassing temperature, humidity, solar radiation and wind speed (Section 4.1). We then explore the magnitude and spatial distribution of biases within a more realistic context (Section 4.2). This is primarily done with ERA5 reanalysis (Hersbach et al., 2018) for a historical period, supplemented by the ACCESS-CM2 model (Dix et al., 2019) for a warmer climate. Afterward, we compare this analytic approximation against other commonly used approximations of WBGT (Section 4.3). Section 5 contains a brief summary and implications on applying WBGT to understanding physical processes controlling heat stress.

2. Liljegren WBGT Model

Here we briefly review the T_g and T_{nw} formulations in Liljegren's WBGT model while directing interested readers to Liljegren et al. (2008) and Kong and Huber (2022) for details.

2.1. Black Globe Temperature

The energy balance equation for the black globe is given by

$$\sigma\epsilon_g T_g^4 + h_{cg}(T_g - T_a) = LR_g + SR_g \tag{2}$$

where energy gain from long-wave (LR_g) and short-wave radiation (SR_g) reaching the globe is balanced by long-wave cooling and energy loss through convective heat transfer between the globe and ambient air corresponding respectively to the two terms on the left side of Equation 2. h_{cg} signifies convective heat transfer coefficient associated with the globe; σ and ϵ_g stand for the Stefan-Boltzmann constant and emissivity of the globe. LR_g

encompasses both downward (LR_{down}) and upwelling thermal radiation (LR_{up}); SR_g also integrates heating from both downward (SR_{down}) and ground surface reflected solar radiation (SR_{up}).

$$LR_g = \frac{1}{2}\epsilon_g (LR_{down} + LR_{up})$$

$$SR_g = \frac{1}{2}(1-\alpha_g)\left[(1-f_{dir})\,SR_{down} + \frac{f_{dir}S_{down}}{2cos(\theta)} + SR_{up}\right]$$

where f_{dir} denotes the fraction of the total horizontal solar irradiance due to the direct beam of the sun; α_g and θ represent globe albedo and solar zenith angle. Note that Liljegren et al. (2008)'s original model only includes SR_{down} as input with other radiation components approximated from air temperature, humidity, ground albedo, etc. However, all radiation components are taken directly from model output in this study (unless otherwise mentioned) as in Kong and Huber (2022).

Equation 2 can be rearranged into

$$T_g = T_a + \frac{SR_g + LR_g - \sigma\epsilon_g T_a^4}{h_{cg} + h_{rg}} \tag{3}$$

where h_{rg} can be interpreted as a thermal radiative heat transfer coefficient

$$h_{rg} = \sigma\epsilon_g\left(T_g^2 + T_a^2\right)(T_g + T_a)$$

$LR_g - \sigma\epsilon_g T_a^4$ is typically small and actually approaches zero when the downward and upward thermal radiation can be represented by a mean radiant temperature of T_a in absence of solar radiation. With this term being neglected, we have

$$T_g - T_a = \frac{SR_g}{h_{cg} + h_{rg}} \tag{4}$$

The physical interpretation of Equation 4 is that the efficiency of energy loss through long-wave cooling (h_{rg}) and convection (h_{cg}) modulates the required temperature gradient between the globe and ambient air in order to balance the energy gain from solar radiation. Note that the simplification in Equation 4 is only meant to aid physical interpretation. Equation 3 will still be used for developing the analytical approximation for the sake of accuracy.

Equation 3 cannot be solved analytically since both h_{cg} and h_{rg} depend nonlinearly on T_g (i.e., Equation 3 is self-nonlinear in T_g). h_{cg} is derived from the empirical correlation for heat transfer from a sphere in cross flow (NIOSH, 1986) (see Eq. 16 in Liljegren et al. (2008) for its formulation). It is mainly affected by wind speed but also depends on air density which is a function of film temperature $\left(T_f\right)$ and surface pressure. T_f is the temperature of the air within the convective boundary layer proximate to the surface of the globe, and is calculated as the arithmetic mean between the temperatures of the globe surface and ambient air $\left(T_f = (T_g + T_a)/2\right)$. Consequently, Equation 3 needs to be solved by iteration to obtain the equilibrium T_g. In Section 3.1, we will provide an analytic solution to T_g which does not require iteration.

2.2. Natural Wet-Bulb Temperature

The energy balance equation for the wick is

$$k_x\frac{e_w - e_a}{P - e_w}M_{H2O}\Delta H + h_{cw}(T_{nw} - T_a) + \sigma\epsilon_w T_{nw}^4 = LR_w + SR_w \tag{5}$$

where the radiative energy gain on the right side of the equation is balanced by energy loss through evaporating water, convection, and thermal radiation corresponding respectively to the three terms on the left side of the

equation. The convective heat transfer coefficient h_{cw} is obtained from the empirical correlation for heat transfer from a cylinder (Bedingfield & Drew, 1950). k_x denotes convective mass transfer coefficient which are interconnected with h_{cw} via the Chilton-Colburn analogy (Chilton & Colburn, 1934). They are both predominantly affected by wind speed with weak dependence on film temperature $\left(T_f = (T_a + T_{nw})/2\right)$ and surface pressure (see Eq. 8 and 10 in Liljegren et al. (2008) for their formulations). e_a and e_w represent ambient vapor pressure and the saturation vapor pressure at the temperature of the wick $(e_w = e_{sat}(T_{nw}))$; P is surface pressure; M_{H2O} is the molecular weight of water vapor; ΔH stands for the heat of vaporization; ϵ_w is the emissivity of the wick. Similar to the case of T_g, SR_w (LR_w) encompasses both downward and upwelling short-wave (long-wave) radiation.

$$LR_w = \frac{1}{2}\epsilon_w (LR_{down} + LR_{up})$$

$$SR_w = (1-\alpha_w)\left[\left(1+\frac{D}{4L}\right)(1-f_{dir})\,SR_{down} + \left(\frac{\tan\theta}{\pi}+\frac{D}{4L}\right)f_{dir}SR_{down} + SR_{up}\right]$$

where α_w, D and L represent the albedo, diameter and length of the wick cylinder.

Equation 5 can be rearranged into

$$T_{nw} = T_a + \frac{SR_w - \beta(e_{sat}(T_a) - e_a) + LR_w - \sigma\epsilon_w T_a^4}{h_{ew} + h_{cw} + h_{rw}} \tag{6}$$

where β is defined as

$$\beta = \frac{k_x M_{H2O}\Delta H}{P - e_w} \approx \frac{k_x M_{H2O}\Delta H}{P}$$

h_{ew} and h_{rw} can be interpreted as evaporative and thermal radiative heat transfer coefficients for the wick cylinder, and are defined as

$$h_{ew} = \beta\frac{e_w - e_{sat}(T_a)}{T_{nw} - T_a} \approx \beta\left.\frac{\partial e_{sat}(T)}{\partial T}\right|_{T=\frac{T_{nw}+T_a}{2}} \tag{7}$$

$$h_{rw} = \sigma\epsilon_w\left(T_{nw}^2 + T_a^2\right)(T_{nw} + T_a)$$

Note that h_{ew}, by definition, measures the efficiency of evaporative heat transfer between the wet wick and a saturated air. The fact that air can be under-saturated creates a cooling term from vapor pressure deficit (VPD) $(\beta(e_{sat}(T_a) - e_a)$ in Equation 6).

With $LR_w - \sigma\epsilon_w T_a^4$ being typically small and neglected, we have

$$T_{nw} - T_a = \frac{SR_w - \beta(e_{sat}(T_a) - e_a)}{h_{ew} + h_{cw} + h_{rw}} \tag{8}$$

Namely, the temperature gradient between the wick and ambient air is driven by net energy input from solar radiation and VPD, regulated by the efficiency of energy loss via evaporation (h_{ew}), convection (h_{cw}) and long-wave cooling (h_{rw}). Equation 8 is only for interpretation purpose and the analytical approximation of T_{nw} is based on Equation 6.

Similar to the case of T_g, Equation 6 needs to be solved by iteration because both the mass transfer (k_x) and three heat transfer coefficients (h_{ew}, h_{cw} and h_{rw}) depend nonlinearly on T_{nw}. An analytic approximation to T_{nw} will be provided in Section 3.2 by removing the self-nonlinearity.

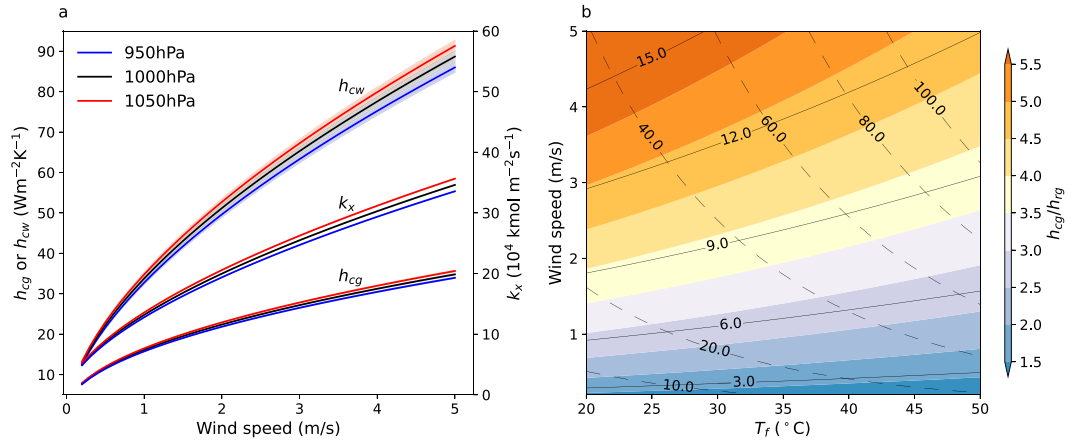

Figure 1. (a) h_{cg}, h_{cw} and k_x as functions of wind speed. Blue, black, and red curves correspond to surface pressure values of 950, 1,000, and 1,050 hPa respectively with the shading represent spread due to film temperature variations from 20 to 50°C. (b) h_{cg}/h_{rg} (shading), h_{cw}/h_{rw} (solid contour) and h_{ew}/h_{rw} (dashed contour) as functions of film temperature and wind speed. Thermal radiative heat transfer coefficients are approximated as $h_{rg} \approx 4\sigma\epsilon_g T_f^3$ for the black globe and $h_{rw} \approx 4\sigma\epsilon_w T_f^3$ for the wet wick, with $\epsilon_g = \epsilon_w = 0.95$. Surface pressure is fixed at 1,000 hPa in panel (b).

3. Analytic Approximation of WBGT

In the previous section, we established that both T_g and T_{nw} cannot be solved analytically because they are embedded nonlinearly within the mass and heat transfer coefficients. Numerical solutions can be pursued through iterative methods: starting with an initial guess, inserting it into the transfer coefficients within Equation 3 or 6, obtaining an updated value, and iteratively repeating this process until consecutive updates deviate by less than a specified tolerance. However, we argue that employing a judicious initial guess might yield a result that is sufficiently accurate, thereby eliminating the need for iterations. By employing this approach, Equations 3 and 6 become analytic formulations of T_g and T_{nw}, and the ensuing solutions are henceforth referred to as analytic approximations.

3.1. Black Globe Temperature

An analytic approximation of T_g can be obtained by substituting a certain first-guess value of T_g into h_{cg} and h_{rg} on the right side of Equation 3. Ideally, the first-guess value should be close to T_g, but this is less critical due to reasons articulated below.

h_{cg} is derived from empirical correlations under forced convection with surrounding fluid motion (Liljegren et al., 2008). It is primarily influenced by wind speed, with minimal impact from variations in film temperature and surface pressure within their typical ranges (Figure 1a). This choice is justified by the dominance of forced convection over free convection under non-negligible wind speeds and reasonable temperature gradients between the globe and ambient air (Gao et al., 2019). Under a wind speed of 2 m/s and surface pressure of 1,000 hPa, a 10°C increase of film temperature from 30 to 40°C only cause a 0.2% reduction in h_{cg}. In fact, the international standard ISO 7726 (ISO, 1998) parameterizes convective heat transfer coefficients under forced convection as solely a function of wind speed. On the other hand, h_{rg} only varies by around 0.5% per °C change in T_g, and energy loss via thermal radiation is typically 2–5 times less efficient than convection (Figure 1b).

The minor influence of temperature on h_{cg} and small fractional changes in h_{rg} with temperature suggest that the initial estimate's proximity to the true value is not critical. Therefore, we choose T_a as a first guess for T_g for simplicity. The resultant approximations to both heat transfer coefficients are denoted as $\widehat{h_{cg}}$ and $\widehat{h_{rg}}$ the latter of which is calculated as $\widehat{h_{rg}} = 4\sigma\epsilon_g T_a^3$. For $\widehat{h_{cg}}$, film temperature is approximated by $T_f = \frac{T_g + T_a}{2} \approx T_a$. Consequently, we have an analytic approximation of T_g:

$$\widehat{T_g} = T_a + \frac{SR_g + LR_g - \sigma\epsilon_g T_a^4}{\widehat{h_{cg}} + \widehat{h_{rg}}} \tag{9}$$

The accuracy of $\widehat{T_g}$ can be assessed by comparing it against the true value of T_g in Equation 3.

$$\widehat{T_g} - T_g = (T_g - T_a)\,\frac{h_{cg} - \widehat{h_{cg}} + h_{rg} - \widehat{h_{rg}}}{\widehat{h_{cg}} + \widehat{h_{rg}}}$$

As explained above, the deviation of $\widehat{h_{cg}}$ from h_{cg} is negligible, which simplifies the bias of $\widehat{T_g}$ into

$$\begin{aligned}\widehat{T_g} - T_g &= (T_g - T_a)\,\frac{h_{rg} - \widehat{h_{rg}}}{\widehat{h_{cg}} + \widehat{h_{rg}}} \\ &= \frac{\sigma\epsilon_g (T_g - T_a)^2\left[(T_g + T_a)^2 + 2T_a^2\right]}{\widehat{h_{cg}} + \widehat{h_{rg}}}\end{aligned} \tag{10}$$

It is clear that $\widehat{T_g}$ always has non-negative biases the magnitude of which is proportional to the square of the temperature gradient between the globe and ambient air. Therefore, $\widehat{T_g}$ is expected to perform better under conditions of weak solar radiation and high wind speed wherein the weaker solar heating and efficient convective heat transfer make T_g closer to T_a. Given T_g and T_a of ~300 K and $T_g - T_a$ of ~20 K, the largest possible bias is ~2 K which can only be realized when $h_{cg} = 0$. However, the actual bias will be significantly smaller since h_{cg} is usually considerably larger than h_{rg} (Figure 1a). The physical interpretation of this formulation is that the approximation to long-wave cooling introduces minimal biases when convection is the dominant pathway for energy loss.

3.2. Natural Wet-Bulb Temperature

An analytic solution for T_{nw} can be obtained by substituting a first-guess value of T_{nw} into the mass and three heat transfer coefficients in Equation 6. Similar to the case of T_g, both k_x and h_{cw} are primarily influenced by wind speed with minor influences from variations in film temperature and surface pressure (Figure 1a). h_{rw} only varies by 0.5% per °C change in T_{nw} and energy loss via thermal radiation is much less efficient than convection and evaporation (Figure 1b). Therefore, the proximity of the first guess to the true T_{nw} is less critical for the coefficients of mass transfer and heat transfer via convection and thermal radiation. However, it might be of greater concern for the evaporative heat transfer coefficient (Equation 7), as h_{ew} varies by around 2%–3% per °C change in T_{nw}, and evaporation is the most efficient energy loss pathway for the wet wick (Figure 1b).

Therefore, a reasonably good first guess for T_{nw} is needed. We choose the wet-bulb temperature (T_w) which is very close to T_{nw} at night and typically remains within 3°C below T_{nw} during the day, depending on solar radiation intensity (Figure 5b). For the sake of computational efficiency and analytic tractability, we calculate T_w from temperature and relative humidity (RH) using an empirical formula developed by Stull (2011). Stull's T_w is subject to around 1°C overestimation at high temperatures, commonly occurring during the day (Buzan et al., 2015). This slight overestimation actually brings Stull's T_w closer to T_{nw} and provides a better initial guess. The resulting analytic approximation is

$$\widehat{T_{nw}} = T_a + \frac{SR_w - \hat{\beta}(e_{sat}(T_a) - e_a) + LR_w - \sigma\epsilon_w T_a^4}{\widehat{h_{ew}} + \widehat{h_{cw}} + \widehat{h_{rw}}} \tag{11}$$

where $\hat{\beta} = \widehat{k_x} M_{H2O}\Delta H/P$. By comparing against Equation 6, we quantify the bias of $\widehat{T_{nw}}$

$$\widehat{T_{nw}} - T_{nw} = \eta(T_{nw} - T_a)\,(T_{nw} - T_w) \tag{12}$$

$$\eta = \frac{\frac{1}{2}\beta \frac{\partial^2 e_{sat}(T)}{\partial T^2}\Big|_{T=\frac{T_{nw}+T_w+2T_a}{4}} + \sigma\epsilon_w\left(T_{nw}^2 + T_w^2 + T_a^2 + T_{nw}T_w + T_aT_{nw} + T_aT_w\right)}{\widehat{h_{ew}} + \widehat{h_{cw}} + \widehat{h_{rw}}}$$

where we assume $\widehat{k_x} \approx k_x$ and $\widehat{h_{cw}} \approx h_{cw}$ since both the convective mass and heat transfer coefficients are extremely insensitive to variations in film temperature (Figure 1a). Since $T_{nw} \geq T_w$, $\widehat{T_{nw}}$ is subject to overestimation when $T_{nw} > T_a$ and underestimation otherwise. By inspection, it is clear that the magnitude of biases increases with enlarging differences between T_{nw} and both T_a and T_w. Over subtropical hot-dry regions, the strong VPD cooling and solar radiative heating are expected to enlarge both temperature gradients with $T_{nw} < T_a$ and $T_{nw} > T_w$ leading to relatively strong negative biases in $\widehat{T_{nw}}$.

3.3. WBGT

Substituting $\widehat{T_g}$ (Equation 9) and $\widehat{T_{nw}}$ (Equation 11) back into Equation 1, we obtain the analytic approximation to WBGT

$$\widehat{WBGT} = 0.7\widehat{T_{nw}} + 0.2\widehat{T_g} + 0.1T_a \tag{13}$$

$\widehat{T_g}$, $\widehat{T_{nw}}$ and $\widehat{WBGT}$ are referred as analytic approximations in the sense that self-nonlinearities in T_g and T_{nw} within the energy balance equations are eliminated by substituting initial estimates of them into the mass and/or heat transfer coefficients. This permits WBGT to be expressed as an analytic function of temperature, humidity, wind and radiation, although this function remains highly complex and nonlinear.

4. Validation of the Analytic Approximation

The validation of the analytic approximation is undertaken in both an idealized and a more realistic context by comparing against results from Liljegren's full model driven by atmospheric variable inputs.

In the idealized setting, we investigate the bias structure of the analytic approximation across a multi-dimensional parameter space of air temperature, wind speed, RH and downward solar radiation based on synthetic data. We highlight the environmental conditions that yield relatively large biases. Note that Liljegren et al. (2008)'s original formulation is used for bias quantification in the idealized setting (Figure 2). Namely, only downward solar radiation is included as input, with other radiation components being approximated. This approach is taken because thermal radiation and surface-reflected solar radiation inherently depend on temperature and downward solar radiation, making it inappropriate to treat these other radiation components as independent dimensions of the climatic phase space.

Next, we examine the magnitude and spatial distribution of biases within a more realistic setting using ERA5 reanalysis (Hersbach et al., 2018) for the period 2013–2022 as inputs. Since we aim to use this approximate framework in a range of climate states, including a much warmer future, we also validate it against a "hot" CMIP6 simulation. This is conducted for the period 2091–2100 under the SSP585 scenario using the ACCESS-CM2 model (Dix et al., 2019) which has a relatively high equilibrium climate sensitivity of 4.7°C (Hausfather, 2019). The data is evaluated at hourly intervals for ERA5 and 3-hourly for ACCESS-CM2 at their original grid spacing. WBGT is calculated from 2 m air temperature and humidity (dewpoint temperature for ERA5 and specific humidity for ACCESS-CM2), 10 m wind speed (transferred to 2 m level), surface pressure, as well as surface downward and upwelling flux of long-wave and short-wave radiation. Direct (diffuse) solar radiation is also retrieved from ERA5 (ACCESS-CM2) to obtain the fraction of direct solar radiation $\left(f_{dir}\right)$.

4.1. Validation and Bias Characterization: Idealized Setting

The accuracy of the analytic approximation is evaluated across a range of air temperature (20–50°C) and wind speed (0.13–3 m/s) under different levels of RH (20% and 60%) and downward solar radiation (0, 450, and 900 W/m^2) (Figure 2).

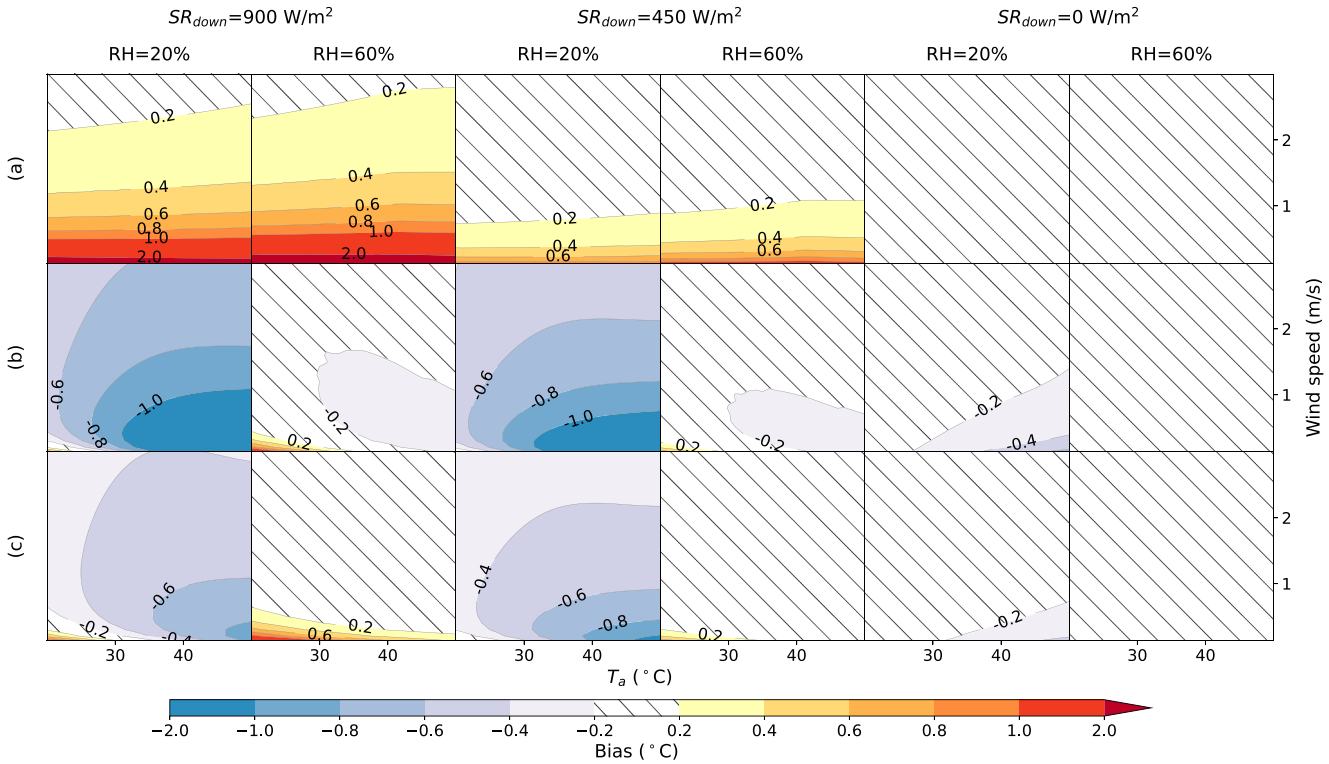

Figure 2. Biases in analytic approximations of (a) T_g, (b) T_{nw}, and (c) wet-bulb globe temperature across the parameter space covering selected ranges of temperature (T_a) (20–50°C), wind speed (0.13–3 m/s), relative humidity (RH) (20%, 60%) and downward solar radiation (SR_{down}) $(0, 450, 900 W/m^2)$. Biases are evaluated against Liljegren's full model. The cosine of the solar zenith angle ($\cos\theta$) is set to 0.75. Thermal radiation, and direct and surface reflected solar radiation are approximated from temperature, RH, $\cos\theta$, SR_{down} and an assumed surface albedo following the original formulation of Liljegren et al. (2008). Surface pressure is fixed at 1,000 hPa.

$\widehat{T_g}$ slightly overestimates T_g in Liljegren's full model by less than 0.2°C during nighttime and under conditions of moderate solar radiation ($450 W/m^2$). However, as solar radiation intensifies and wind speed diminishes, the degree of overestimation becomes more pronounced. It can exceed 1°C under scenarios of strong solar radiation ($900\ W/m^2$) and low wind speed ($<0.5 m/s$) (Figure 2a). This intensification of overestimation can be attributed to the increased temperature gradient between the black globe and the ambient air (as illustrated in Equation 10) due to intense solar heating and less effective energy loss through convection under low wind speed. In practice, the relatively large overestimation under low wind speed is less a concern as the movement of human body creates relative air flow especially for outdoor workers. In fact, prior studies frequently assume a minimum wind speed of 1 m/s when assessing heat stress-induced labor loss (Bröde et al., 2018; Casanueva et al., 2020; Kjellstrom et al., 2018).

$\widehat{T_{nw}}$ has small biases (within ±0.2°C of T_{nw} in Liljeren's full model) at nighttime when T_w, our initial estimate, is close to T_{nw} (Figure 5b). At daytime, $\widehat{T_{nw}}$ performs well under wet condition (60% RH). However, under dry condition (20% RH), $\widehat{T_{nw}}$ shows substantial underestimations especially under lower wind speed and higher temperature where the underestimation can extend up to −2°C. This can be attributed to a strong temperature gradient between the wet wick and the ambient air $(T_{nw} - T_a)$ under hot-dry conditions with low wind speed (as illustrated in Equation 12). The underestimation also intensifies under stronger solar radiation probably owing to an enlarged difference between T_{nw} and T_w.

Biases in $\widehat{WBGT}$ are expected to be primarily influenced by biases in $\widehat{T_{nw}}$, given that T_{nw} contributes 70% to WBGT. Accordingly, we found that $\widehat{WBGT}$ shares a similar bias structure with $\widehat{T_{nw}}$, but the magnitudes are smaller and within ±0.8°C across the selected ranges of meteorological conditions (Figure 2c).

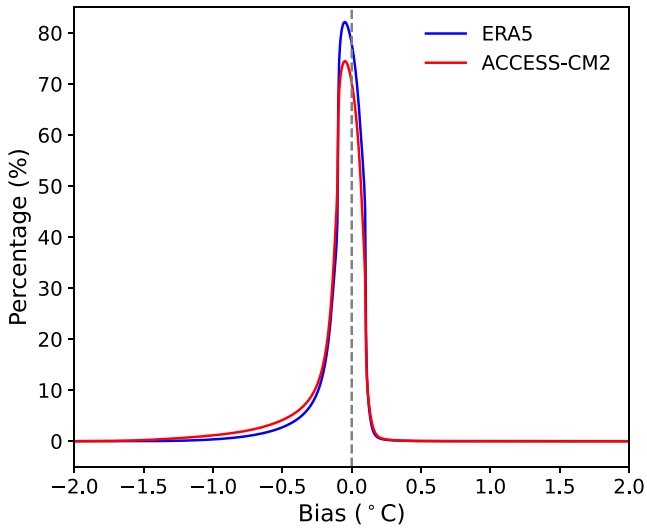

Figure 3. Empirical probability distribution of biases in our analytic approximation $\widehat{WBGT}$. The *y*-axes are designed to represent the percentage of samples showing biases within a 0.2°C interval centered on the corresponding x coordinates. The empirical distribution is derived from land data weighted by grid-cell area using ERA5 reanalysis for the period 2013–2022 and the ACCESS-CM2 model for the period 2091–2100 under the SSP585 scenario. Samples with wet-bulb globe temperature below 15°C are excluded, as they are less relevant to heat stress.

4.2. Validation and Bias Characterization: Realistic Setting

The bias characterization within the idealized setting demonstrates the structure of biases in the analytic approximations across a range of meteorological conditions. In practice, those meteorological conditions are not equally sampled with some combinations of temperature, humidity, solar radiation and/or wind speed more or less likely. It is of interest to examine the likely magnitudes and spatial distribution of biases in more realistic settings.

Figure 3 shows the area-weighted empirical distribution of biases in $\widehat{WBGT}$ over land. During the period 2013–2022 of ERA5, around 78% of the total samples have biases within ±0.1°C, while this percentage extends to 97% for biases within ±0.5°C. A similar level of accuracy is maintained in a warmer world with 93% of samples falling within ±0.5°C. Although the peak of the distribution around zero becomes lower, accompanied by a slightly fatter tail on the side of negative biases (Figure 3), it is unclear whether this accuracy reduction can be attributed to climate change (Sherwood & Huber, 2010; Williams et al., 2009), or due to potential effects from other confounding factors such as the distinct spatial resolutions between ERA5 and ACCESS-CM2. For our purpose however, the method is sufficiently accurate across a wide range of climates.

Using ERA5, we then highlight the annual 1% and 99% percentile of these biases, thereby directing attention to the tails of the bias distribution and their spatial patterns (Figure 4). $\widehat{T}_g$, as demonstrated in Equation 10, is only subject to overestimations the 1% percentile of which is close to zero (Figure 4a). The 99% percentile of the overestimations is within 1°C over 97% of global land area (Figures 4b and 4k). Over some alpine areas, like the Himalayas, strong solar radiation stemming from an optically thin atmosphere leads to large disparities between T_g and T_a, thereby causing relatively strong overestimations (>1.8°C) (Figure 4b).

In comparison, $\widehat{T_{nw}}$, can cause both under- and overestimations. The 1% percentile of biases is characterized by underestimations within −1°C over 85% of land area (Figures 4d and 4j). Over subtropical dry regions, strong VPD and solar radiation make T_{nw} substantially smaller than T_a and larger than T_w which induces more pronounced underestimations by $\widehat{T_{nw}}$ (Figure 4d) as demonstrated in Equation 12. The 99% percentile of biases show weak overestimations within 0.6°C over 92% of land area (Figures 4e and 4k). Over the Himalayas alpine region, small VPD (as a result of cold temperature) and strong solar radiation make T_{nw} considerably larger than both T_a and T_w leading to relatively strong overestimations (Figure 4e).

$\widehat{WBGT}$ shares a similar spatial distribution of biases as $\widehat{T_{nw}}$ with the 1% percentile of biases showing underestimations within −1°C over 96% of land area (Figures 4g and 4j), and the 99% percentile characterized by overestimations within 0.6°C over 94% of land area (Figures 4h and 4k).

We also show the 99% percentile of the absolute values of biases in the analytic approximations (Figures 4c, 4f, 4i, and 4l) in order to highlight the upper tail of the magnitudes of their deviations from Liljegren's full model. In 99% cases, biases in $\widehat{T}_g$, $\widehat{T_{nw}}$ and $\widehat{WBGT}$ are limited within ±1°C over 97%, 82%, and 93% of land area. It is also of interest to know the performance of our analytic approximation in representing heat stress at the levels of annual mean and different percentiles. As shown in Figures 6q–6t, $\widehat{WBGT}$ can well represent heat stress across annual mean and 75%, 90% and 99% percentiles with biases within ±0.5°C globally.

4.3. Comparison Against Other Approximations

We compare $\widehat{WBGT}$ against several other WBGT approximations commonly used in the literature. These include sWBGT which only contains temperature and humidity while implicitly assuming moderately strong solar radiation and low wind speeds (Australian Bureau of Meteorology, 2010), the environmental stress index (ESI), derived through a multivariate regression of WBGT against temperature, downward solar radiation, and RH (Moran et al., 2001, 2003), the indoor WBGT ($WBGT_{in}$) which substitutes T_{nw} with the thermodynamic wet-bulb

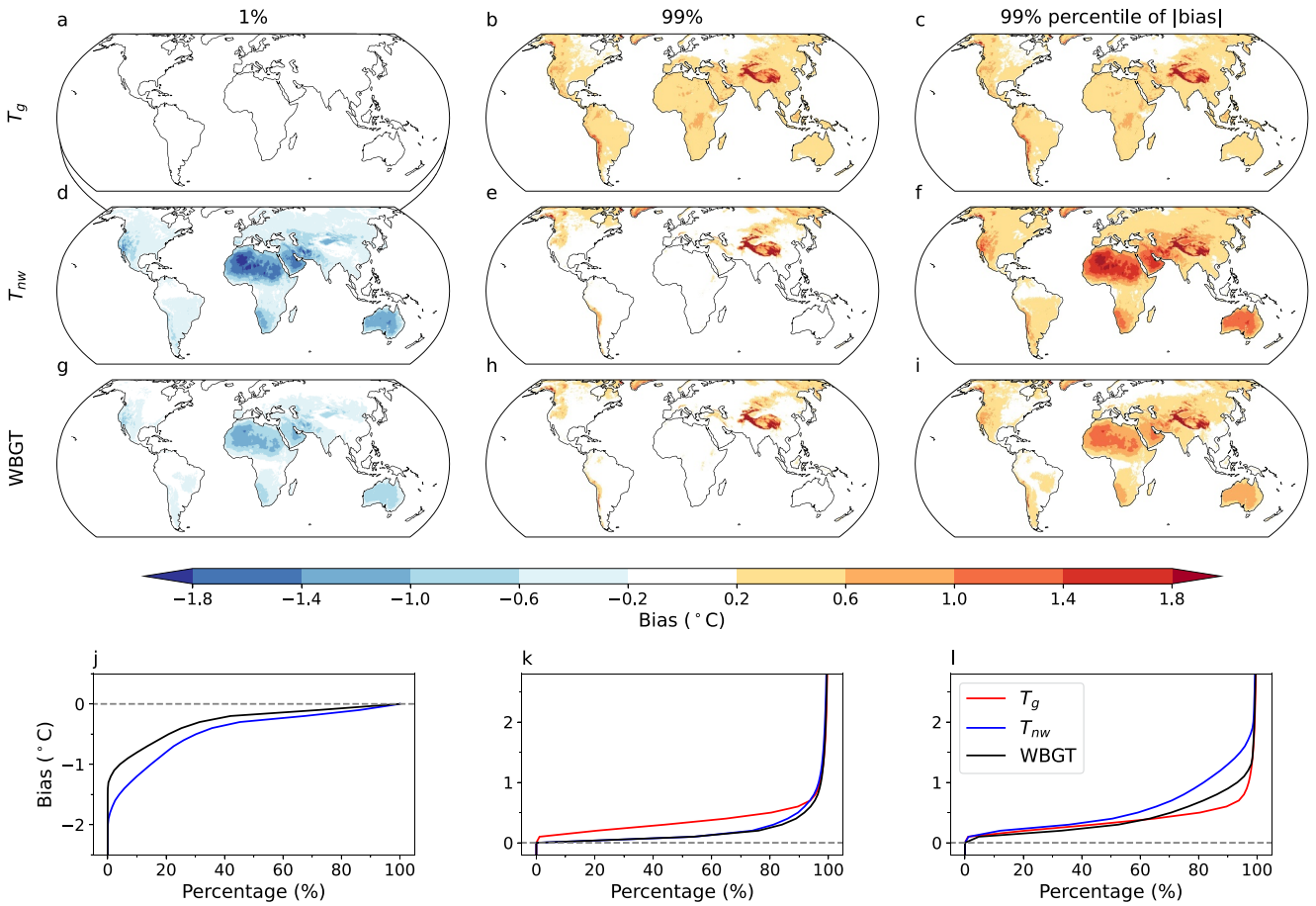

Figure 4. Annual (left) 1% and (middle) 99% percentile of biases, and (right) 99% percentile of the absolute magnitudes of biases in the analytic approximations of (a–c) T_g, (d–f) T_{nw} and (g–i) wet-bulb globe temperature. Panels j–l represent the empirical cumulative distribution of these biases across all continental grid cells weighted by area. The 1% percentile of biases in $\widehat{T_g}$ are very close to zero and therefore are omitted in (j). Biases are evaluated by comparing against Liljegren's full model based on hourly ERA5 reanalysis data during 2013–2022.

temperature (T_w) and T_g with T_a (Dunne et al., 2013; C. Li et al., 2020; D. Li et al., 2020), and the one recently developed by Brimicombe et al. (2023) ($WBGT_{Br}$) which calculates T_g from mean radiant temperature, and approximates T_{nw} using Stull's T_w formulation (Stull, 2011).

Figure 5a illustrates the empirical bias distribution of these approximations along with that of our analytic approximation based on ERA5. $\widehat{WBGT}$ clearly outperforms others. *sWBGT* performs the worst, and its bias distribution peaks at an overestimation of approximately 5°C potentially due to the implicit assumption of moderately strong solar radiation and low wind. This overestimate can profoundly affect future heat stress projections and estimate of impact on people (de Lima et al., 2021; Sun et al., 2024; Zhang & Shindell, 2021; Zhu et al., 2021). Therefore, we do not recommend the continued use of sWBGT. ESI performs significantly better with a relatively symmetric distribution of biases centered around zero.

The distribution of biases in both $WBGT_{in}$ and $WBGT_{Br}$ have a primary peak near zero as well as secondary peaks corresponding to underestimations of approximately −2.4 and −1.2°C respectively (Figure 5a). Both $WBGT_{in}$ and $WBGT_{Br}$ substitute T_{nw} with T_w, and $WBGT_{in}$ also approximates T_g with T_a. These approximations work relatively well during nighttime especially for T_{nw} (Figure 5b). Notably, T_g is lower than T_a at nighttime, and the distribution of their differences peaks around −1°C, but can extend up to −3°C (Figure 5b). That is because air is not a black body, and consequently the long-wave radiative exchange between the black globe and ambient air produce net cooling on the globe. However, during daytime, T_w and T_a significantly underestimate T_{nw} and T_g due to the omission of solar radiative heating. The distributions of these underestimations peak around −1.2 and

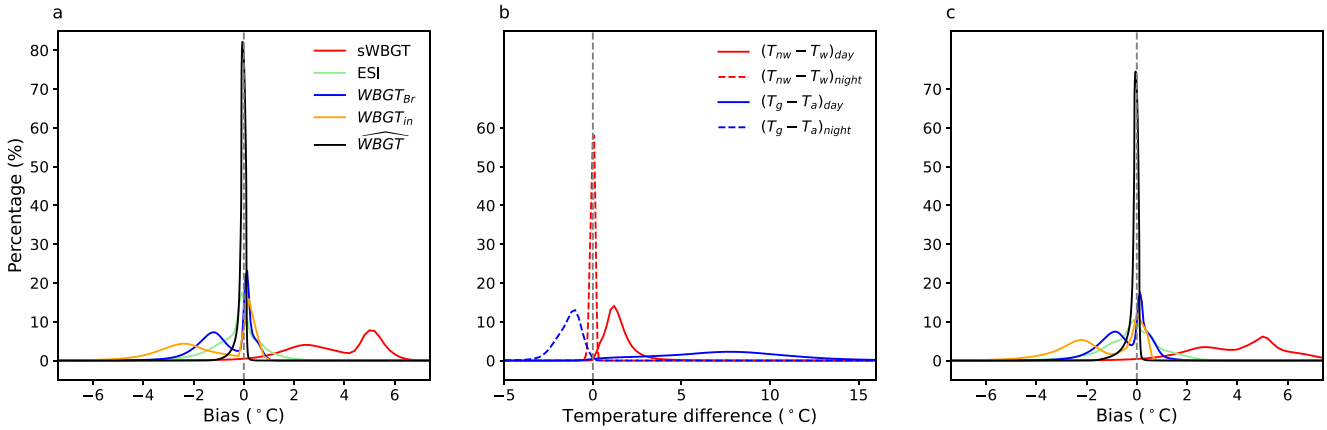

Figure 5. Empirical probability distribution of (a) biases in our analytic formulation $\widehat{WBGT}$ and several other wet-bulb globe temperature (WBGT) approximations, and (b) $T_{nw}-T_w$ and T_g-T_a at both daytime and nighttime. Both (a) and (b) are derived from land data weighted by grid-cell area using ERA5 reanalysis for the period of 2013–2022. Panel (c) is the same as (a) except for the period 2091–2100 under the SSP585 scenario using the ACCESS-CM2 model. The *y*-axes are designed to represent the percentage of samples showing biases within a 0.2°C interval centered on the corresponding x coordinates. Samples with WBGT below 15°C are excluded, as they are less relevant to heat stress.

−7.6°C respectively (Figure 5b) which amounts to underestimations in WBGT of −0.8 and −1.5°C given the weights on T_{nw} and T_g in WBGT formulation. The differentiated daytime versus nighttime performances explain the bimodal distribution of biases in $WBGT_{in}$ and $WBGT_{Br}$ (Figure 5a).

The shape of the bias distribution and the relative performance of different approximations remain consistent in a future warmer world, where $\widehat{WBGT}$ continues to have the best performance (Figure 5c).

Our analytic approximation also performs better in representing the annual mean and 75%–99% percentiles of WBGT. The biases are within ±0.1°C in the majority of regions, and mostly within ±0.5°C except over the Sahara and Arabian deserts and alpine areas in the Tibetan Plateau for higher percentiles (Figure 6). sWBGT strongly overestimates WBGT especially at annual mean level, and this overestimation becomes weaker toward higher percentiles where the assumption of moderately strong solar radiation becomes more applicable (Figures 6a–6d). ESI performs well in capturing annual mean and 75% percentile of WBGT with biases mostly within ±1°C, but considerably underestimates the 99% percentile by up to −4°C across the low latitudes (Figures 6e–6h). Both $WBGT_{in}$ and $WBGT_{Br}$ consistently show underestimations the magnitude of which increases toward higher percentiles (Figures 6i–6p). Among them, $WBGT_{Br}$ has better performance since T_g is calculated from mean radiant temperature rather than replaced with T_a as is done for $WBGT_{in}$.

5. Summary and Implication

We have developed an approximate form of WBGT that does not require iterative calculation. The need for iteration in WBGT calculation arises from the nonlinear dependence of mass and/or heat transfer (through convection, thermal radiation and evaporation) efficiencies on T_g or T_{nw}, rendering the energy balance equations analytically intractable. However, we have shown that this dependence is weak for convection which is primarily influenced by wind speed. This self-dependence is also of minor importance for thermal radiation because the thermal radiative heat transfer coefficient changes by a small fraction within the typical variation range of T_g or T_{nw}, and energy loss via thermal radiation is much less efficient than convection and evaporation. The dependence of evaporative heat transfer coefficient on T_{nw} is of greater concern since h_{ew} is relatively sensitive to T_{nw} variations (h_{ew} varies by 2%–3% per °C change in T_{nw}) and evaporation plays a dominant role in the energy loss of the wet wick.

The recognition of the weak self-nonlinearity, at least for convection and thermal radiation, motivates the development of an analytic approximation of WBGT by substituting T_a and T_w as initial estimates for T_g and T_{nw} into the mass and heat transfer coefficients. The analytic approximation eliminates the need for iteration and is more accurate than other WBGT approximations commonly used in the literature. It presents an useful first guess to Liljegren's full model given its reasonably high accuracy and computational straightforwardness. However,

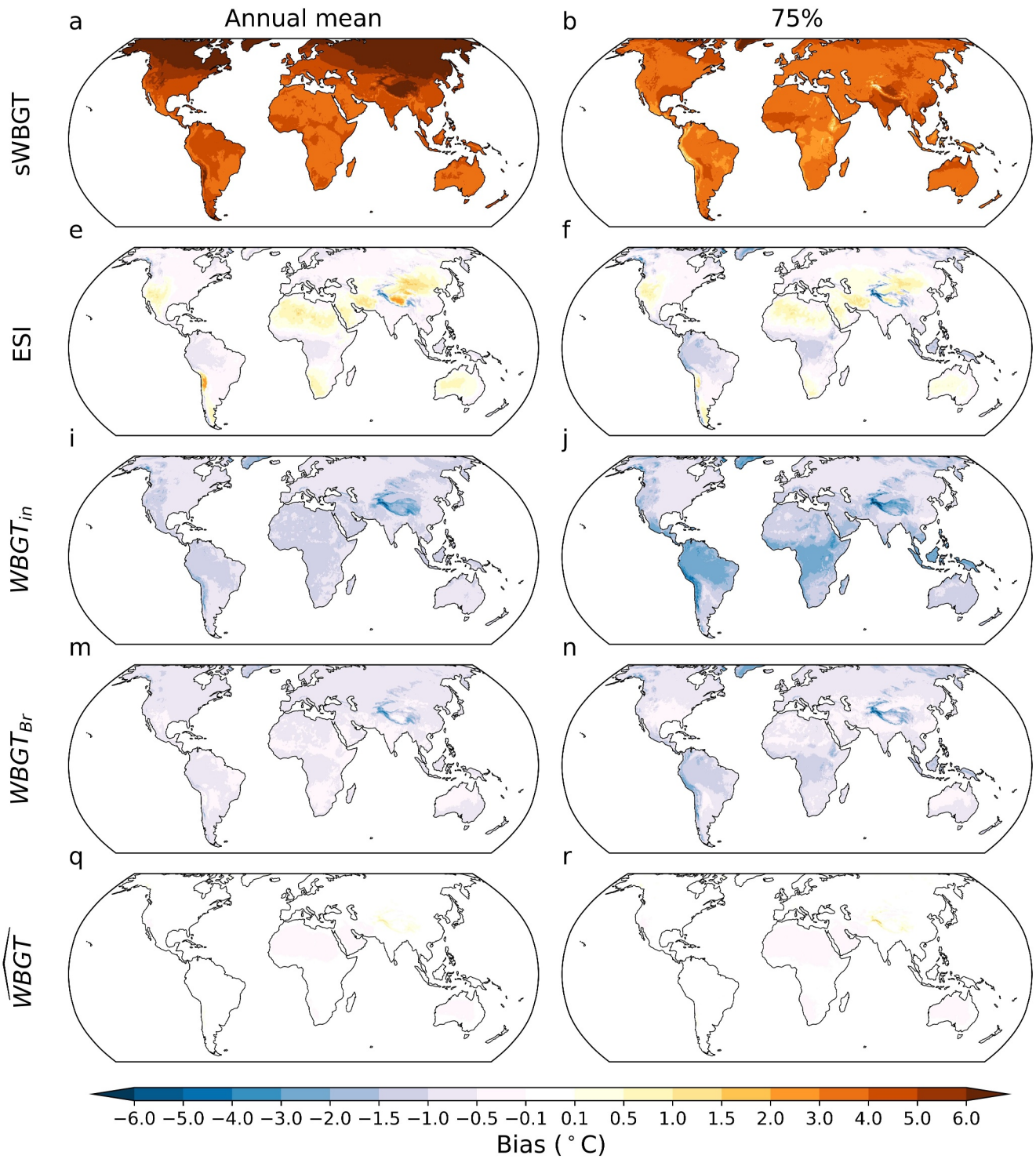

Figure 6. Biases in the (a, e, i, m, q) annual mean and (b, f, j, n, r) 75%, (c, g, k, o, s in Figure 6 continued) 90%, and (d, h, l, p, t in Figure 6 continued) 99% percentile values of our analytic approximation $\widehat{WBGT}$ and several other approximations of wet-bulb globe temperature. Biases are evaluated by comparing against Liljegren's full model based on hourly ERA5 reanalysis data during 2013–2022.

10.1029/2024GH001068

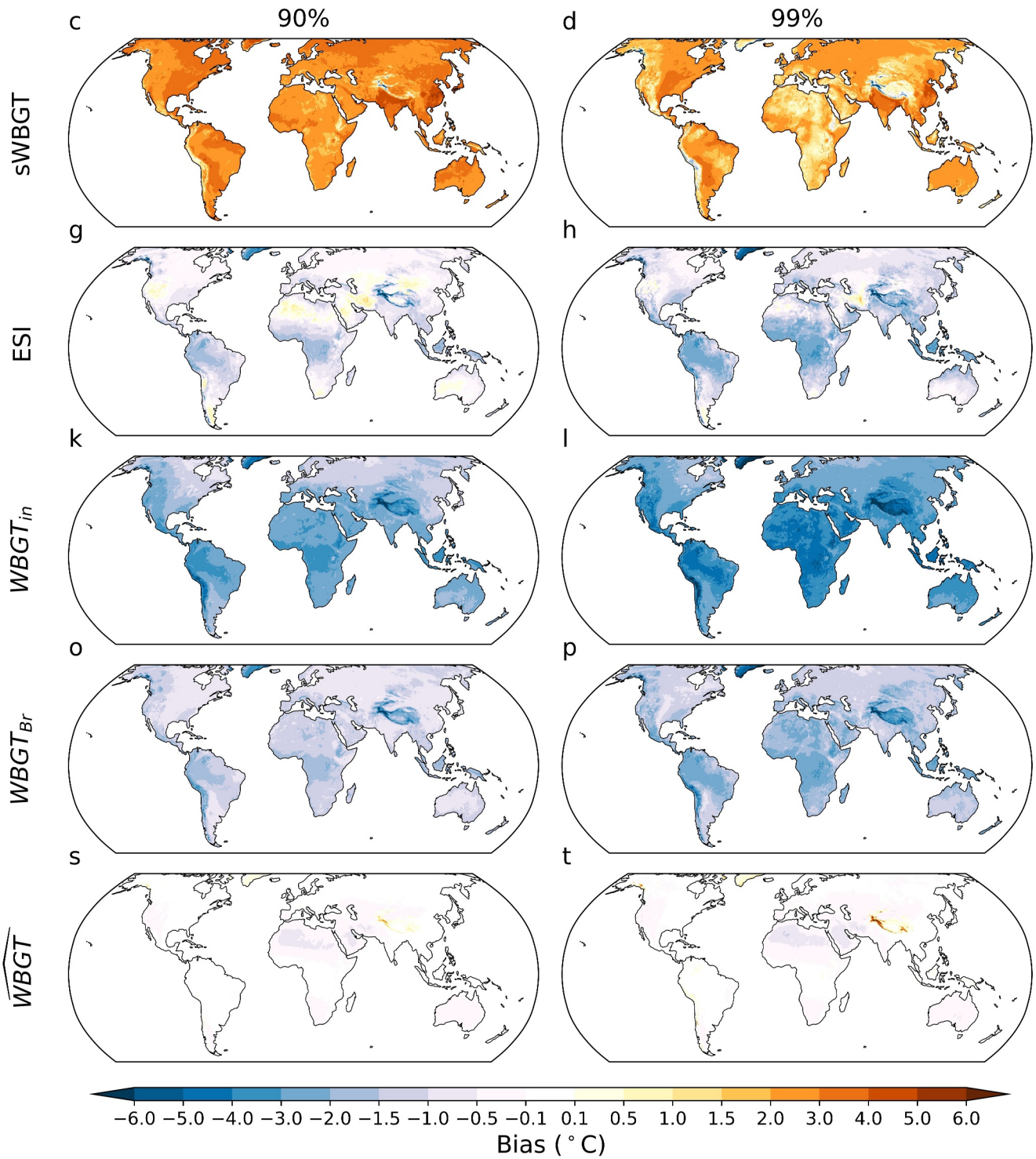

Figure 6. (Continued)

users should consider the potential underestimation of heat stress under extremely hot-dry conditions. Notably, more accurate estimates can be obtained through a single iteration, with the analytic approximations serving as the updated first guesses. Recently, Liljeren's WBGT formulation has been implemented into the Community Land Model Version 5 (CLM5) for non-urban settings (Buzan, 2024). Our analytic approximation could offer an useful

alternative for inclusion in the model to prevent the model from slowing down due to iterative WBGT calculations.

The complex, nonlinear interactions between multiple meteorological parameters not only require WBGT to be calculated iteratively, but also lead to a functional form that is opaque to theoretical investigation and often times treated as a black box. As a result, WBGT–despite being a good representation of human heat stress–has not been adopted for understanding the atmospheric dynamics and thermodynamic processes controlling heat stress. Instead, strictly thermodynamic variables like T_w, moist enthalpy or equivalent potential temperature are used for such purpose because of their straightforward dynamic and thermodynamic constraint (Kong & Huber, 2023; Lutsko, 2021; Raymond et al., 2021; Zhang et al., 2021). But these thermodynamic quantities are not intended for or well calibrated to human heat stress which diminishes the practical relevance of the generated insights (Lu & Romps, 2023; Simpson et al., 2023).

In deriving the analytic approximation, we have gained insights that the deviation of both T_g and T_{nw} from T_a is controlled by the ratio between solar radiative heating (and VPD cooling for T_{nw}) and the efficiency of energy loss through convection and long-wave cooling (and evaporation for T_{nw}) (Equations 4 and 8). Therefore, understanding changes in T_g, T_{nw} and consequently WBGT, must involve strong constraints or knowledge of the evolution of this ratio. Depending on the problem under consideration, if solar radiation and wind speed remain unchanged, the ratio for T_g (Equation 4) is approximately constant given minor influence from changes in thermal radiative heat transfer efficiency. Consequently, T_g is expected to vary at the same rate as T_a. It is less straightforward to get a quick, simple relation between changes in T_{nw} and T_a, as the ratio in Equation 8 also depends on humidity and T_{nw} itself due to the VPD cooling term and evaporative heat transfer coefficient. Nevertheless, given certain assumptions on humidity changes (e.g., constant RH), we should be able to explicitly predict how T_{nw} scales with temperature as well. In addition, since T_{nw} is driven away from T_w by solar radiation under the modulation of wind, we may expect the differences between them to be roughly constant if both solar radiation and wind remain unchanged. If this is the case, the scaling of T_{nw} and T_w with temperature should be close to each other.

More generally, Equations 4 and 8, with their clear physical interpretation, may serve as a starting point for an analytic investigation of the sensitivity of WBGT to changes in temperature, humidity, wind and solar radiation. Clearly, we have better intuition on these traditional meteorological parameters, and established theories to constrain their variations (Byrne, 2021; Byrne & O'Gorman, 2013, 2016; McColl & Tang, 2024; Zhang & Boos, 2023). An explicit, analytic expression of WBGT's sensitivity to these traditional meteorological variables helps remove the obscuring veil of WBGT's apparent complexity and may facilitate its application in understanding the physical control of heat stress. For example, we can quantitatively disentangle the relative role of changes in each meteorological input and the underlying physical processes in explaining WBGT responses to any physical perturbations (like atmospheric blocking events, irrigation or increasing greenhouse gas emission).

Conflict of Interest

The authors declare no conflicts of interest relevant to this study.

Data Availability Statement

Hersbach et al. (2018) was downloaded from the Copernicus Climate Change Service (C3S) Climate Data Store (https://cds.climate.copernicus.eu/cdsapp#!/dataset/reanalysis-era5-single-levels?tab=form). The results contain modified Copernicus Climate Change Service information 2020. Neither the European Commission nor ECMWF is responsible for any use that may be made of the Copernicus information or data it contains. Dix et al. (2019) was downloaded from https://esgf-index1.ceda.ac.uk/search/cmip6-ceda/. Liljegren's WBGT code in C language is accessible at https://github.com/mdljts/wbgt/blob/master/src/wbgt.c, and was ported to Cython (can be compiled and implemented in Python) by Kong and Huber (2022) (available at https://zenodo.org/record/5980536). The code for the analytic WBGT approximation is deposited at Zenodo (https://zenodo.org/records/10802580) along with a Jupyter notebook to introduce its usage. $WBGT_{in}$ was calculated using the code developed by D. Li et al. (2020) (available at https://github.com/dw-li/WBGT) while correcting the inappropriate humidity approximations identified by Rogers and Warren (2024). $WBGT_{Br}$ was calculated using the thermofeel Python package (available at https://github.com/ecmwf/thermofeel/tree/master) (Brimicombe et al., 2021, 2022), with

the mean radiant temperature retrieved from ERA5-HEAT (Di Napoli, 2020; Di Napoli et al., 2021) (available at https://cds.climate.copernicus.eu/cdsapp#!/dataset/derived-utci-historical?tab=form). The following Python packages were also utilized: Numpy (Harris et al., 2020), Xarray (Hoyer & Hamman, 2017), Dask (Dask Development Team, 2016), Matplotlib (Hunter, 2007), and Cartopy (Met Office, 2010–2015).

Acknowledgments
This study is Funded by NASA FINESST Grant 80NSSC22K1544, Grant NSF 1805808-CBET Innovations at the Nexus of Food, Energy, and Water Systems (INFEWS: U.S.-China): A multi-scale integrated modeling approach to managing the transition to sustainability and NSF 1829764-OAC CyberTraining: CIU: Cross-disciplinary Training for Findable, Accessible, Interoperable, and Reusable (FAIR) science. We thank Rodrigo Caballero for useful discussions that clarified the presentation of concepts in this study.

References

ACSM. (1984). *Position stand on the prevention of thermal injuries during distance running*. (Technical Report). Medicine & Science in Sports & Exercise.

Army, U. (2003). Heat stress control and heat casualty management (Technical Report). *Technical Bulletin Medical 507/Air Force Pamphlet*.

Australian Bureau of Meteorology. (2010). About the approximation to the WBGT used by the Bureau of Meteorology. Retrieved from http://www.bom.gov.au/info/thermal_stress/#approximation

Bedingfield, C. H., & Drew, T. B. (1950). Analogy between heat transfer and mass transfer. *Industrial & Engineering Chemistry*, *42*(6), 1164–1173. https://doi.org/10.1021/ie50486a029

Brimicombe, C., Di Napoli, C., Quintino, T., Pappenberger, F., Cornforth, R., & Cloke, H. (2021). thermofeel [Software]. *European Centre for Medium-Range Weather Forecasts*. https://doi.org/10.21957/MP6V-FD16

Brimicombe, C., Di Napoli, C., Quintino, T., Pappenberger, F., Cornforth, R., & Cloke, H. L. (2022). Thermofeel: A python thermal comfort indices library [Software]. *SoftwareX*, *18*, 101005. https://doi.org/10.1016/j.softx.2022.101005

Brimicombe, C., Lo, C. H. B., Pappenberger, F., Di Napoli, C., Maciel, P., Quintino, T., et al. (2023). Wet bulb globe temperature: Indicating extreme heat risk on a global grid. *GeoHealth*, *7*(2), e2022GH000701. https://doi.org/10.1029/2022GH000701

Bröde, P., Fiala, D., Lemke, B., & Kjellstrom, T. (2018). Estimated work ability in warm outdoor environments depends on the chosen heat stress assessment metric. *International Journal of Biometeorology*, *62*(3), 331–345. https://doi.org/10.1007/s00484-017-1346-9

Budd, G. M. (2008). Wet-bulb globe temperature (WBGT)—Its history and its limitations. *Journal of Science and Medicine in Sport*, *11*(1), 20–32. https://doi.org/10.1016/j.jsams.2007.07.003

Burke, M., González, F., Baylis, P., Heft-Neal, S., Baysan, C., Basu, S., & Hsiang, S. (2018). Higher temperatures increase suicide rates in the United States and Mexico. *Nature Climate Change*, *8*(8), 723–729. https://doi.org/10.1038/s41558-018-0222-x

Burke, M., Hsiang, S. M., & Miguel, E. (2015). Global non-linear effect of temperature on economic production. *Nature*, *527*(7577), 235–239. https://doi.org/10.1038/nature15725

Buzan, J. R. (2024). Implementation and evaluation of wet bulb globe temperature within non-urban environments in the community land model version 5. *Journal of Advances in Modeling Earth Systems*, *16*(2), e2023MS003704. https://doi.org/10.1029/2023MS003704

Buzan, J. R., & Huber, M. (2020). Moist heat stress on a hotter Earth. *Annual Review of Earth and Planetary Sciences*, *48*(1), 623–655. https://doi.org/10.1146/annurev-earth-053018-060100

Buzan, J. R., Oleson, K., & Huber, M. (2015). Implementation and comparison of a suite of heat stress metrics within the Community Land Model version 4.5. *Geoscientific Model Development*, *8*(2), 151–170. https://doi.org/10.5194/gmd-8-151-2015

Byrne, M. P. (2021). Amplified warming of extreme temperatures over tropical land. *Nature Geoscience*, *14*(11), 837–841. https://doi.org/10.1038/s41561-021-00828-8

Byrne, M. P., & O'Gorman, P. A. (2013). Land–ocean warming contrast over a wide range of climates: Convective quasi-equilibrium theory and idealized simulations. *Journal of Climate*, *26*(12), 4000–4016. https://doi.org/10.1175/JCLI-D-12-00262.1

Byrne, M. P., & O'Gorman, P. A. (2016). Understanding decreases in land relative humidity with global warming: Conceptual model and GCM simulations. *Journal of Climate*, *29*(24), 9045–9061. https://doi.org/10.1175/JCLI-D-16-0351.1

Casanueva, A., Kotlarski, S., Fischer, A. M., Flouris, A. D., Kjellstrom, T., Lemke, B., et al. (2020). Escalating environmental summer heat exposure—A future threat for the European workforce. *Regional Environmental Change*, *20*(2), 40. https://doi.org/10.1007/s10113-020-01625-6

Chavaillaz, Y., Roy, P., Partanen, A.-I., Da Silva, L., Bresson, E., Mengis, N., et al. (2019). Exposure to excessive heat and impacts on labour productivity linked to cumulative CO_2 emissions. *Scientific Reports*, *9*(1), 13711. https://doi.org/10.1038/s41598-019-50047-w

Chilton, T. H., & Colburn, A. P. (1934). Mass transfer (absorption) coefficients prediction from data on heat transfer and fluid friction. *Industrial & Engineering Chemistry*, *26*(11), 1183–1187. https://doi.org/10.1021/ie50299a012

Clark, J., & Konrad, C. E. (2023). Observations and estimates of wet bulb globe temperature in varied microclimates. *Journal of Applied Meteorology and Climatology*, *63*(2), 305–319. https://doi.org/10.1175/JAMC-D-23-0078.1

Dask Development Team. (2016). Dask: Library for dynamic task scheduling [Software]. *Computer software manual*. Retrieved from https://dask.org

de Freitas, C. R., & Grigorieva, E. A. (2015). A comprehensive catalogue and classification of human thermal climate indices. *International Journal of Biometeorology*, *59*(1), 109–120. https://doi.org/10.1007/s00484-014-0819-3

de Lima, C. Z., Buzan, J. R., Moore, F. C., Baldos, U. L. C., Huber, M., & Hertel, T. W. (2021). Heat stress on agricultural workers exacerbates crop impacts of climate change. *Environmental Research Letters*, *16*(4), 044020. https://doi.org/10.1088/1748-9326/abeb9f

Di Napoli, C. (2020). Thermal comfort indices derived from ERA5 reanalysis [Dataset]. *ECMWF*. https://doi.org/10.24381/CDS.553B7518

Di Napoli, C., Barnard, C., Prudhomme, C., Cloke, H. L., & Pappenberger, F. (2021). ERA5-HEAT: A global gridded historical dataset of human thermal comfort indices from climate reanalysis [Dataset]. *Geoscience Data Journal*, *8*(1), 2–10. https://doi.org/10.1002/gdj3.102

Dix, M., Bi, D., Dobrohotoff, P., Fiedler, R., Harman, I., Law, R., et al. (2019). CSIRO-ARCCSS ACCESS-CM2 model output prepared for CMIP6 ScenarioMIP ssp585 [Dataset]. *Earth System Grid Federation*. https://doi.org/10.22033/ESGF/CMIP6.4332

Dunne, J. P., Stouffer, R. J., & John, J. G. (2013). Reductions in labour capacity from heat stress under climate warming. *Nature Climate Change*, *3*(6), 563–566. https://doi.org/10.1038/nclimate1827

Ebi, K. L., Capon, A., Berry, P., Broderick, C., De Dear, R., Havenith, G., et al. (2021). Hot weather and heat extremes: Health risks. *The Lancet*, *398*(10301), 698–708. https://doi.org/10.1016/S0140-6736(21)01208-3

Foster, J., Smallcombe, J. W., Hodder, S., Jay, O., Flouris, A. D., & Havenith, G. (2022a). Quantifying the impact of heat on human physical work capacity; part II: The observed interaction of air velocity with temperature, humidity, sweat rate, and clothing is not captured by most heat stress indices. *International Journal of Biometeorology*, *66*(3), 507–520. https://doi.org/10.1007/s00484-021-02212-y

Foster, J., Smallcombe, J. W., Hodder, S., Jay, O., Flouris, A. D., Nybo, L., & Havenith, G. (2022b). Quantifying the impact of heat on human physical work capacity; part III: The impact of solar radiation varies with air temperature, humidity, and clothing coverage. *International Journal of Biometeorology*, *66*(1), 175–188. https://doi.org/10.1007/s00484-021-02205-x

Gao, J., Wang, Y., Wu, X., Gu, X., & Song, X. (2019). A simplified indoor wet-bulb globe temperature formula to determine acceptable hot environmental parameters in naturally ventilated buildings. *Energy and Buildings*, *196*, 169–177. https://doi.org/10.1016/j.enbuild.2019.05.035

Harris, C. R., Millman, K. J., van der Walt, S. J., Gommers, R., Virtanen, P., Cournapeau, D., et al. (2020). Array programming with NumPy [Software]. *Nature*, *585*(7825), 357–362. https://doi.org/10.1038/s41586-020-2649-2

Hausfather, Z. (2019). CMIP6: The next generation of climate models explained. Retrieved from https://www.carbonbrief.org/cmip6-the-next-generation-of-climate-models-explained

Havenith, G., & Fiala, D. (2015). Thermal indices and thermophysiological modeling for heat stress. In R. Terjung (Ed.), *Comprehensive physiology* (pp. 255–302). John Wiley & Sons, Inc. https://doi.org/10.1002/cphy.c140051

Havenith, G., Smallcombe, J. W., Hodder, S., Jay, O., & Foster, J. (2024). Comparing efficacy of different climate indices for predicting labor loss, body temperature, and thermal perception in a wide variety of warm and hot climates. *Journal of Applied Physiology*, *137*(2), 312–328. https://doi.org/10.1152/japplphysiol.00613.2023

Hersbach, H., Bell, B., Berrisford, P., Biavati, G., Horányi, A., Muñoz Sabater, J., et al. (2018). ERA5 hourly data on single levels from 1979 to present [Dataset]. *Copernicus Climate Change Service (C3S) Climate Data Store (CDS)*. https://doi.org/10.24381/cds.adbb2d47

Hoyer, S., & Hamman, J. (2017). xarray: N-D labeled arrays and datasets in Python [Software]. *Journal of Open Research Software*, *5*(1), 10. https://doi.org/10.5334/jors.148

Hsiang, S. M., Burke, M., & Miguel, E. (2013). Quantifying the influence of climate on human conflict. *Science*, *341*(6151), 1235367. https://doi.org/10.1126/science.1235367

Hunter, J. D. (2007). Matplotlib: A 2D graphics environment [Software]. *Computing in Science & Engineering*, *9*(3), 90–95. https://doi.org/10.1109/MCSE.2007.55

Ioannou, L. G., Tsoutsoubi, L., Mantzios, K., Vliora, M., Nintou, E., Piil, J. F., et al. (2022). Indicators to assess physiological heat strain – Part 3: Multi-country field evaluation and consensus recommendations. *Temperature*, *9*(3), 274–291. https://doi.org/10.1080/23328940.2022.2044739

ISO. (1998). *Ergonomics of the thermal environment - instruments for measuring physical quantities (International Standard)*. International Organization for Standardization (ISO).

ISO. (2017). *Ergonomics of the thermal environment — Assessment of heat stress using the WBGT (wet bulb globe temperature) index (International Standard)*. International Organization for Standardization (ISO).

Kamal, A. S. M. M., Faruki Fahim, A. K., & Shahid, S. (2024). Simplified equations for wet bulb globe temperature estimation in Bangladesh. *International Journal of Climatology*, *44*(5), 1636–1653. https://doi.org/10.1002/joc.8402

Kjellstrom, T., Briggs, D., Freyberg, C., Lemke, B., Otto, M., & Hyatt, O. (2016). Heat, human performance, and occupational health: A key issue for the assessment of global climate change impacts. *Annual Review of Public Health*, *37*(1), 97–112. https://doi.org/10.1146/annurev-publhealth-032315-021740

Kjellstrom, T., Freyberg, C., Lemke, B., Otto, M., & Briggs, D. (2018). Estimating population heat exposure and impacts on working people in conjunction with climate change. *International Journal of Biometeorology*, *62*(3), 291–306. https://doi.org/10.1007/s00484-017-1407-0

Kong, Q., & Huber, M. (2022). Explicit calculations of wet bulb globe temperature compared with approximations and why it matters for labor productivity. *Earth's Future*, *10*(3), e2021EF002334. https://doi.org/10.1029/2021EF002334

Kong, Q., & Huber, M. (2023). Regimes of soil moisture-wet bulb temperature coupling with relevance to moist heat stress. *Journal of Climate*, *36*(22), 1–45. https://doi.org/10.1175/JCLI-D-23-0132.1

Lemke, B., & Kjellstrom, T. (2012). Calculating workplace WBGT from meteorological data: A tool for climate change assessment. *Industrial Health*, *50*(4), 267–278. https://doi.org/10.2486/indhealth.MS1352

Li, C., Sun, Y., Zwiers, F., Wang, D., Zhang, X., Chen, G., & Wu, H. (2020). Rapid warming in summer wet bulb globe temperature in China with human-induced climate change. *Journal of Climate*, *33*(13), 5697–5711. https://doi.org/10.1175/JCLI-D-19-0492.1

Li, D., Yuan, J., & Kopp, R. E. (2020). Escalating global exposure to compound heat-humidity extremes with warming. *Environmental Research Letters*, *15*(6), 064003. https://doi.org/10.1088/1748-9326/ab7d04

Liljegren, J. C., Carhart, R. A., Lawday, P., Tschopp, S., & Sharp, R. (2008). Modeling the wet bulb globe temperature using standard meteorological measurements. *Journal of Occupational and Environmental Hygiene*, *5*(10), 645–655. https://doi.org/10.1080/15459620802310770

Lu, Y.-C., & Romps, D. (2023). Wet-bulb temperature or heat index: Which better predicts fatal heat in a warming climate? *Physiology*, *38*(S1), 5734524. https://doi.org/10.1152/physiol.2023.38.S1.5734524

Lutsko, N. J. (2021). The relative contributions of temperature and moisture to heat stress changes under warming. *Journal of Climate*, *34*(3), 901–917. https://doi.org/10.1175/JCLI-D-20-0262.1

Matsumoto, K., Tachiiri, K., & Su, X. (2021). Heat stress, labor productivity, and economic impacts: Analysis of climate change impacts using two-way coupled modeling. *Environmental Research Communications*, *3*(12), 125001. https://doi.org/10.1088/2515-7620/ac3e14

McColl, K. A., & Tang, L. I. (2024). An analytic theory of near-surface relative humidity over land. *Journal of Climate*, *37*(4), 1213–1230. https://doi.org/10.1175/JCLI-D-23-0342.1

Met Office. (2010–2015). Cartopy: A cartographic python library with a matplotlib interface [Software]. *Computer software manual*. Retrieved from https://scitools.org.uk/cartopy

Moran, D., Pandolf, K., Laor, A., Heled, Y., Matthew, W., & Gonzalez, R. (2003). Evaluation and refinement of the environmental stress index for different climatic conditions. *Journal of Basic and Clinical Physiology and Pharmacology*, *14*(1), 1–16. https://doi.org/10.1515/JBCPP.2003.14.1.1

Moran, D., Pandolf, K., Shapiro, Y., Heled, Y., Shani, Y., Mathew, W., & Gonzalez, R. (2001). An environmental stress index (ESI) as a substitute for the wet bulb globe temperature (WBGT). *Journal of Thermal Biology*, *26*(4–5), 427–431. https://doi.org/10.1016/S0306-4565(01)00055-9

NIOSH. (1986). *Criteria for a recommended standard—occupational exposure to hot environments* (Technical Report No. DHHS/NIOSH Pub. No. 86-113). Department of Health and Human Services (DHHS), National Institute for Occupational Safety and Health (NIOSH).

NIOSH. (2016). *Criteria for a recommended standard: Occupational exposure to heat and hot environments* (Technical Report No. DHHS (NIOSH) Publication No. 2016-106). DHHS, NIOSH.

Orlov, A., De Hertog, S., Havermann, F., Guo, S., Luo, F., Manola, I., et al. (2023). Changes in land cover and management affect heat stress and labor capacity. *Earth's Future*, *11*(3), e2022EF002909. https://doi.org/10.1029/2022EF002909

OSHA. (2017). *OSHA Technical Manual, Section III, Chapter 4: Heat stress*. (Technical Report No. TED-01-00-015). U.S. Department of Labor, OSHA: Occupational Safety and Health Administration (OSHA).

Patel, T., Mullen, S. P., & Santee, W. R. (2013). Comparison of methods for estimating wet-bulb globe temperature index from standard meteorological measurements. *Military Medicine*, *178*(8), 926–933. https://doi.org/10.7205/MILMED-D-13-00117

Raymond, C., Matthews, T., Horton, R. M., Fischer, E. M., Fueglistaler, S., Ivanovich, C., et al. (2021). On the controlling factors for globally extreme humid heat. *Geophysical Research Letters*, *48*(23), e2021GL096082. https://doi.org/10.1029/2021GL096082

Rogers, C. D. W., & Warren, R. A. (2024). Fast and accurate calculation of wet-bulb temperature for humid-heat extremes. *Authorea Preprints*. https://doi.org/10.22541/essoar.170560423.39769387/v1

Saeed, W., Haqiqi, I., Kong, Q., Huber, M., Buzan, J. R., Chonabayashi, S., et al. (2022). The poverty impacts of labor heat stress in West Africa under a warming climate. *Earth's Future*, *10*(11), e2022EF002777. https://doi.org/10.1029/2022EF002777

Sherwood, S. C., & Huber, M. (2010). An adaptability limit to climate change due to heat stress. *Proceedings of the National Academy of Sciences*, *107*(21), 9552–9555. https://doi.org/10.1073/pnas.0913352107

Simpson, C. H., Brousse, O., Ebi, K. L., & Heaviside, C. (2023). Commonly used indices disagree about the effect of moisture on heat stress. *npj Climate and Atmospheric Science*, *6*(1), 78. https://doi.org/10.1038/s41612-023-00408-0

Stull, R. (2011). Wet-bulb temperature from relative humidity and air temperature. *Journal of Applied Meteorology and Climatology*, *50*(11), 2267–2269. https://doi.org/10.1175/JAMC-D-11-0143.1

Sun, Y., Zhu, S., Wang, D., Duan, J., Lu, H., Yin, H., et al. (2024). Global supply chains amplify economic costs of future extreme heat risk. *Nature*, *627*(8005), 797–804. https://doi.org/10.1038/s41586-024-07147-z

Tuholske, C., Caylor, K., Funk, C., Verdin, A., Sweeney, S., Grace, K., et al. (2021). Global urban population exposure to extreme heat. *Proceedings of the National Academy of Sciences*, *118*(41), e2024792118. https://doi.org/10.1073/pnas.2024792118

Vecellio, D. J., Wolf, S. T., Cottle, R. M., & Kenney, W. L. (2022). Utility of the Heat Index in defining the upper limits of thermal balance during light physical activity (PSU HEAT Project). *International Journal of Biometeorology*, *66*(9), 1759–1769. https://doi.org/10.1007/s00484-022-02316-z

Williams, I. N., Pierrehumbert, R. T., & Huber, M. (2009). Global warming, convective threshold and false thermostats. *Geophysical Research Letters*, *36*(21), L21805. https://doi.org/10.1029/2009GL039849

Yaglou, C. P., & Minard, D. (1957). Control of heat casualties at military training centers. *A.M.A. Archives of Industrial Health*, *16*(4), 302–316.

Zhang, Y., & Boos, W. R. (2023). An upper bound for extreme temperatures over midlatitude land. *Proceedings of the National Academy of Sciences*, *120*(12), e2215278120. https://doi.org/10.1073/pnas.2215278120

Zhang, Y., Held, I., & Fueglistaler, S. (2021). Projections of tropical heat stress constrained by atmospheric dynamics. *Nature Geoscience*, *14*(3), 133–137. https://doi.org/10.1038/s41561-021-00695-3

Zhang, Y., & Shindell, D. T. (2021). Costs from labor losses due to extreme heat in the USA attributable to climate change. *Climatic Change*, *164*(3–4), 35. https://doi.org/10.1007/s10584-021-03014-2

Zhu, J., Wang, S., Zhang, B., & Wang, D. (2021). Adapting to changing labor productivity as a result of intensified heat stress in a changing climate. *GeoHealth*, *5*(4), e2020GH000313. https://doi.org/10.1029/2020GH000313